The Recombination of Propargyl Radicals: Solving the Master Equation

James A. Miller* and Stephen J. Klippenstein

Combustion Research Facility, Sandia National Laboratories, Livermore, California 94551-0969

Received: January 26, 2001; In Final Form: May 21, 2001

We have investigated theoretically the recombination reaction between two propargyl (C_3H_3) radicals using previously published BAC-MP4 calculations (supplemented by DFT-B3LYP results) to characterize the potential energy surface, RRKM theory to compute microcanonical rate coefficients, and solutions to the time-dependent, multiple-well master equation to predict thermal rate coefficients and product distributions as a function of temperature and pressure. The thermal rate coefficient $k(T,p)$ drops off precipitously at high temperature, regardless of the pressure. Below 500 K, $k(T,p) \approx k_\infty(T)$, the high-pressure limit rate coefficient for initial complex formation, independent of p. For 500 K < T < 2000 K, the rate coefficient increases with increasing pressure, as one would normally expect. At 2000 K, the "coalescence temperature" for this reaction, $k(T,p) = k_0(T)$, the zero-pressure rate coefficient, and only bimolecular products (phenyl + H) are predicted, *no matter how high we make the pressure*. The latter effect is a consequence of all the intermediate complexes reaching their "stabilization limits," a concept discussed extensively in the text. Below 800 K, many C_6H_6 isomers are formed as products, and the pressure and temperature dependence of the branching fractions is easily understood from conventional reasoning. Above 800 K, the product distributions begin to be dominated by isomers reaching their stabilization limits and disappearing as important products. Above 1200 K, the only significant products are fulvene, benzene, and phenyl + H. Beyond 1700 K fulvene disappears, and for T > 2000 K the only products are phenyl + H. We discuss our results in terms of the eigenvalues and eigenvectors of G, the transition matrix of the master equation. A "good" rate coefficient exists only when the rate is controlled by a single eigenvalue of G. A jump of the $k(T,p)$ curve for any pressure from one eigenvalue to another is triggered by the reaching of critical stabilization limits, producing "avoided crossings" of the eigenvalue curves. It is at such avoided crossings that biexponential reactant decays occur.

Introduction

Resonantly stabilized free radicals (RSFR's) are generally believed to play a critical role in the formation of aromatic compounds, polycyclic aromatic compounds, and soot in the combustion of hydrocarbon fuels.[1−25] The unpaired electron in such radicals is delocalized and spread out over two or more sites in the molecule, resulting in at least two corresponding resonant electronic structures of comparable importance. As a result of the delocalization of the unpaired electron, resonantly stabilized free radicals normally form weaker bonds than do ordinary radicals, particularly with stable molecules[1,22,23,26,27] (perhaps most notably with molecular oxygen). Such weakly bound addition complexes are not easily stabilized by collisions at high temperature, nor do they readily support rearrangement. Consequently, RSFR's are relatively unreactive and can reach high concentrations in flames. These high concentrations and the relatively rapid rates at which one RSFR may react with another make RSFR + RSFR reactions an important mechanism for building higher hydrocarbons in flames.

The simplest and most important RSFR, at least from a combustion chemistry point of view, is propargyl (C_3H_3), which has the two resonant Kekulé structures, the first of which is

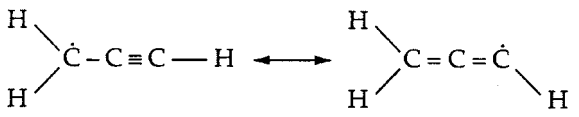

dominant. Although other reactions may make important contributions under certain conditions, the reaction between two propargyl radicals,

$$C_3H_3 + C_3H_3 \rightarrow \text{products} \qquad \text{(R1)}$$

is generally believed to be the single most important cyclization step in flames of aliphatic fuels.[1,2−4,8−10,16−24,28,29] Moreover, many other RSFR's postulated to be important in the cyclization and PAH growth processes are simply radical-substituted propargyls,[1,17,18] e.g., 1-methylallenyl (CH_3CCCH_2). Therefore, it is extremely important to understand the mechanism of reaction (R1) in some detail, particularly the extent to which it may form cyclic products such as benzene, fulvene, and phenyl + H.

The theoretical prediction of the rate coefficient and product distribution of the C_3H_3 + C_3H_3 reaction is a daunting task. However, this reaction has a number of important features that are likely to be typical of reactions involved in higher hydrocarbon growth in flames. First, the two propargyl radicals can collide in three different ways, forming three chemically distinct collision complexes. Each of these complexes may in turn rearrange to form any one of a number of other complexes (corresponding to different isomers of C_6H_6) with no intrinsic energy barrier. A further complication is that all of the accessible complexes live long enough to suffer numerous collisions under normal conditions.[1] Moreover, for reasons discussed extensively in a previous article,[1] simple approximations to the collisional

10.1021/jp0102973 CCC: $20.00
Published on Web 07/07/2001

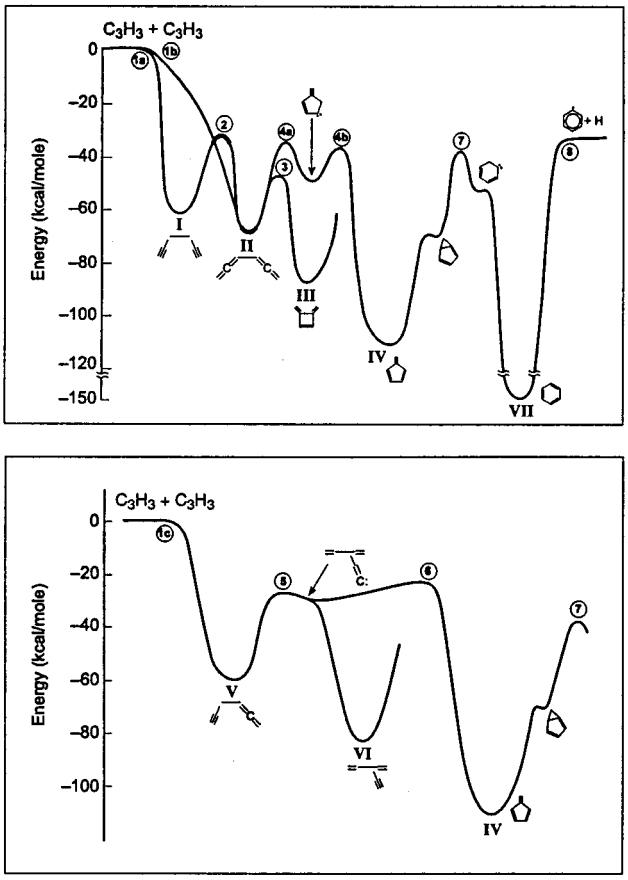

Figure 1. Potential energy diagram for the recombination of two propargyl radicals. Part (a) is for head-to-head and tail-to-tail recombination; part (b) is for head-to-tail recombination.

stabilization process, such as strong-collider or pseudo strong-collider models, are not likely to produce accurate rate coefficients and product distributions. There appears to be no reasonable alternative but to seek solutions to the full multiple-well master equation.

The present article describes such a master-equation approach to the propargyl + propargyl recombination reaction. We make use of the BAC-MP4 potential energy surface (PES) of Miller and Melius[22] and Melius et al.[23] throughout, even though several modifications have suggested themselves during the course of the analysis. For the present, we restrict ourselves simply to determining the consequences of the BAC-MP4 potential. These results should provide a convenient point of departure for future work, pointing out where more experiments and refinements to the potential are needed.

Theory

Potential Energy Surface. The potential energy surface on which the present analysis is based is depicted diagrammatically in Figure 1. As mentioned in the Introduction, the energies of all the stationary points, including the separated fragments, come from BAC-MP4 electronic structure calculations,[22,23] even though subsequent work on various aspects of the C_6H_6 potential[30−34] may need to be taken into account in future work. However, we did replace the less accurate Hartree−Fock vibrational frequencies and rotational constants that come out of the BAC-MP4 method with our own density functional (DFT-B3LYP/6-31G*) calculations of these quantities.

Figure 1 is separated into 2 parts: Figure 1a shows the C_6H_6 isomers that can result from head-to-head and tail-to-tail recombination of the two propargyl radicals (the head is the CH_2 end and the tail is the CH end of propargyl), and Figure 1b shows those that can form from head-to-tail recombination. Both reaction paths go through fulvene (well IV), and the subsequent fulvene → benzene isomerization and benzene → phenyl + H dissociation are common to the two paths. The BAC-MP4 calculations[22,23] show several other C_6H_6 isomers that may be formed from $C_3H_3 + C_3H_3$ with no intrinsic energy barrier; however, these isomers are energetically less accessible than the ones shown in the diagram by at least 25 kcal/mol. Consequently, we have neglected them in the present analysis. Such an approximation substantially reduces the strain on our computing resources.

The Loose Transition States. Figure 1 shows four "loose" transition states, i.e., states with no energy barrier in the exothermic direction. These bond-breaking (bond-forming) processes correspond to the formation from propargyl + propargyl of 1,5-hexadiyne (TS-1a), 1, 2, 4, 5-hexatetraene (TS-1b), and 1, 2-hexadiene-5-yne (TS-1c), and to the dissociation of benzene to form phenyl + H (TS-8). There is no information currently available for these regions of the PES, and it is beyond the scope of the present work to calculate such potentials from first principles. To do so correctly requires the use of relatively sophisticated multireference methods. Rather, we have chosen to approximate these parts of the potential in the manner described by Miller and Klippenstein.[35]

For each of the loose transition states, the potential is divided into three parts. (1) *The potential along the reaction coordinate.* This part of the potential is approximated by the Varshni function.[35,36] The Varshni potential is similar to a Morse potential except that it is "flatter" at large bond distances, and thus it is likely to be a more accurate representation of real bonding potentials than is the Morse function. The two parameters in the Varshni potential are calculated from the BAC-MP4 bond energy and from the force constant matrix at the potential minimum. The latter comes from a DFT-B3LYP/6−31G* calculation and contains $V_{RR}(R_o)$, the second derivative of the potential with respect to the distance R between the bonding atoms at the potential minimum, which is used to determine the Varshni β_v. (2) *The potential for the "conserved" degrees of freedom orthogonal to the reaction coordinate*. The second contribution to the potential corresponds to the degrees of freedom that can be identified as normal-mode vibrations in the separated fragments and is assumed to be the same as in those fragments. Such an assumption is motivated by the observation that variationally determined transition states for bond-breaking reactions usually lie at relatively large values of R. (3) *The potential for the "transitional" degrees of freedom orthogonal to the reaction coordinate*. This last piece of the potential is described in terms of a set of internal angles and is written essentially as a sum of products (in pairs) of sinusoidal functions whose phases and periods are determined by symmetry (see eq 4 of ref 35). The coefficients in the expression are functions of R, and their values are derived from the force constant matrix discussed above. This matrix is calculated only at $R = R_o$, and the required matrix elements are assumed to decay exponentially with the distance between the bonding atoms,

$$F_{ij}(R) = F_{ij}(R_o)\exp[-\eta(R - R_o)] \qquad (1)$$

The tightening (or loosening) parameter η is treated as an adjustable constant for each transition state. Their values are chosen to give rate coefficients that are consistent with low-temperature kinetics experiments.

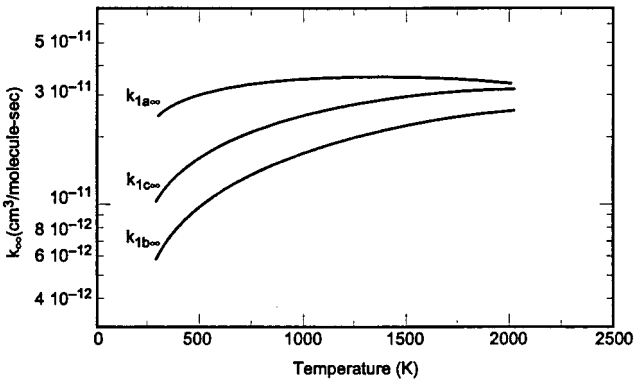

Figure 2. Rate coefficients $k_{1a\infty}(T)$, $k_{1b\infty}(T)$, and $k_{1c\infty}(T)$ corresponding to the three different ways two propargyl radicals can come together.

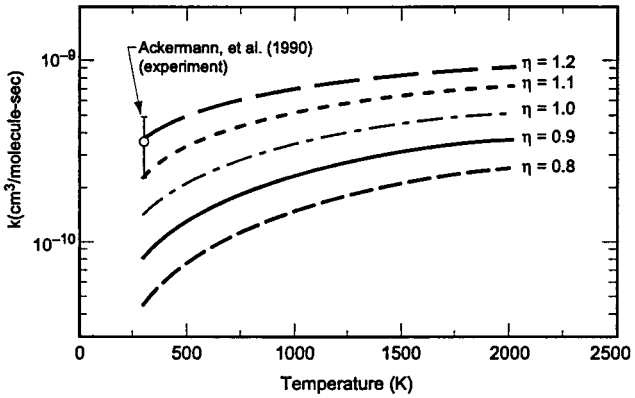

Figure 3. Rate coefficient $k_{8\infty}(T)$ for various values of η_8, the tightening parameter for TS-8. The experimental result is due to Ackermann et al.[70]

To determine appropriate η values, we calculate the "high-pressure limit" rate coefficients $k_{i\infty}$ for each of the transition states (i = 1a, 1b, 1c, 8) using microcanonical, J-resolved variational transition state theory (μVT-J).[1,37−39] Such rate coefficients are given by the expression

$$k_{i\infty} = \frac{1}{hQ_{\mathrm{Rm}}(T)} \int_0^\infty \left[\sum_J (2J+1) N_i^{\pm}(E, J)\right] \exp(-\beta E)\, \mathrm{d}E \quad (2)$$

where $\beta = (k_B T)^{-1}$, T is the temperature, k_B is Boltzmann's constant, h is Planck's constant, E is the total internal energy, Q_{Rm} is the reactant partition function (including relative translational contributions), J is the total angular momentum quantum number, and $N_i^{\pm}(E, J)$ is the sum of states with energy less than or equal to E and total angular momentum quantum number equal to J. For i = 1a, 1b, and 1c, the reactants are taken to be two propargyl radicals, but for i = 8 the reactants are phenyl + H (in the latter case, of course, the energy scale in eq 2 is shifted appropriately).

Fahr and Nayak[40] have determined both the total rate coefficient k and product distribution of the $C_3H_3 + C_3H_3$ reaction at T = 295 K and a pressure of p = 50 Torr. They give $k = 4.0 \times 10^{-11}$ cm^3/molecule-s, with $\alpha_I = 0.60$ and $\alpha_v = 0.25$, where α_I and α_v are the branching fractions for stabilization into well I and well V, respectively. They also detected a third C_6H_6 isomer, of unknown identity, whose formation accounts for 15% of the reaction. This information yields three independent rate coefficients that we equate with $k_{1a\infty}$, $k_{1c\infty}$, and $k_{1b\infty}$ at T = 295 K. The values of η_{1a}, η_{1b}, and η_{1c} are adjusted to give these rate coefficients in our analysis. The assumption that the total rate coefficient is in the high-pressure limit under these conditions is justified by the results presented below. However, the assumption about the product distribution implicit in this procedure neglects the possibility that the complexes formed initially from $C_3H_3 + C_3H_3$ can rearrange and be stabilized as some other isomer under the experimental conditions of Fahr and Nayak. Nevertheless, the assumption we have made is the most objective a priori choice that we have at our disposal. Furthermore, the relative ordering of the rate coefficients matches expectations based on the dominance of the propargyl resonance structure with the unpaired electron on the CH_2 site. The room-temperature product distribution is discussed below. Figure 2 shows the calculated values of $k_{1a\infty}(T)$, $k_{1b\infty}(T)$, and $k_{1c\infty}(T)$ consistent with our assumptions.

Figure 3 shows values of $k_{8\infty}(T)$ for various values of η_8. Also shown on the plot is the single direct experimental value for the phenyl + H rate coefficient of which we are aware. We have chosen in our analysis to use a value of η_8 = 0.9, even though the theoretical value of $k_{8\infty}$ using this value of η_8 lies below the experimental rate coefficient. This choice was made for two reasons: (1) We expected that the formation of phenyl + H from $C_3H_3 + C_3H_3$ might be a controversial result, and we wanted to be somewhat conservative in our prediction for this channel. Of course, larger values of $k_{8\infty}$ lead to larger values of the branching fraction to phenyl + H, everything else being equal. (2) The functional form we use to represent bond-breaking potentials (all three parts) generally leads to rate coefficients that increase with temperature. This may or may not be correct. Such rate coefficients could remain constant or decrease slightly with increasing temperature. The present choice of η_8 = 0.9 results in values of $k_{8\infty}(T)$ for $T \geq 1000$ K that are just slightly smaller than the experimental room-temperature value.

Microcanonical Rate Coefficients, State Counting, and Hindered Rotors. Under the constraints of the RRKM approximation, any one of the dissociation or isomerization processes depicted in Figure 1 can be described in terms of a microcanonical rate coefficient $k(E)$

$$k(E) = \frac{N_j^{\pm}(E)}{h\rho_i(E)} \quad (3)$$

where $N_j^{\pm}(E)$ is the sum of states for transition state j with energy less than or equal to E, and $\rho_i(E)$ is the density of states per unit energy for isomer i, i.e., the ith well in Figure 1. The μVT-J approach[1,37−39] is used in the present analysis to calculate $N_j^{\pm}(E, J)$ for the loose transition states, and conventional transition-state theory is employed for the tight ones. In either case, $N_j^{\pm}(E)$ and $\rho_i(E)$ are computed from sums over J, $N_j^{\pm}(E) = \sum_J (2J+1) N_j^{\pm}(E, J)$, $\rho_i(E) = \sum_J (2J+1)\rho_i(E, J)$. The present problem formulation does not rigorously conserve angular momentum. An angular momentum conserving approach would require the solution of a two-dimensional master equation, and such solutions for a problem as complex as this one are well beyond our current resources. However, the use of μVT-J to calculate $k(E)$ for the loose transition states incorporates some important angular momentum effects into the calculation.

There are two exceptions to the above discussion. Transition state 4 (TS-4) consists of two saddle points with a relatively shallow well in between, too shallow for any significant stabilization to occur. Consequently, we approximate $N_4^{\pm}(E)$ as $N_{4a}^{\pm} N_{4b}^{\pm} / (N_{4a}^{\pm} + N_{4b}^{\pm})$, which assumes that the well is deep enough for the RRKM assumption to apply, but not deep enough to support stabilization. There is another, even shallower, well

in Figure 1b between transition states 5 and 6. However, there is no significant barrier between this well and well VI. Consequently, we effectively subsume it into well VI, taking TS-5 to connect well V directly with well VI and TS-6 to connect well VI directly with well IV, even though the shallow carbene well is an intermediate in both cases. The shallow carbene well makes a contribution to the density of states of the two wells combined that is negligible compared with that of well VI.

The sums and densities of states, N(E,J) and ρ(E,J), are computed rigorously in the present investigation by methods described previously,[35,41−44] normally in the harmonic-oscillator rigid-rotor approximation. However, some "vibrational" degrees of freedom are not described accurately as harmonic oscillators. The most common of these are torsional motions, in the present case rotations about C−C single bonds. These are modeled in the present analysis as hindered rotors, and their sums and densities of states are calculated by methods discussed in some detail in previous publications.[35,41,42]

The computer code VARIFLEX,[45] written by Klippenstein and co-workers, is used in all the calculations described here.

The Master Equation. To determine the rate coefficient $k(T,p)$ and product distribution for the propargyl + propargyl recombination reaction, we must consider the time-dependent, multiple-well master equation.[41−43,46−56] In our analysis, such an equation is cast in the form of seven coupled integro-differential equations:

$$\frac{\mathrm{d}n_i(E)}{\mathrm{d}t} = Z\int_{E_{0i}}^{\infty} P_i(E,E')n_i(E')\,\mathrm{d}E' - Zn_i(E) - \sum_{j\neq i}^{M} k_{ji}(E)n_i(E) + \sum_{j\neq i}^{M} k_{ij}(E)n_j(E) - k_{\mathrm{d}i}(E)n_i(E) + K_{\mathrm{eq}i}k_{\mathrm{d}i}(E)F_i(E)n_{\mathrm{R}}n_m - k_{pi}(E)n_i(E) \quad (i = I, ..., M) \quad (4)$$

In these equations, t is the time, Z is the collision number per unit time, $n_i(E)\ dE$ is the number density of molecules (or complexes) in well i with energy between E and $E + \mathrm{d}E$, E_{0i} is the ground-state energy for well i, M is the number of wells (seven (VII) in the present case), $P_i(E,E')$ is the probability that a molecule in well i with energy between E' and $E' + \mathrm{d}E'$ will be transferred by collision to a state with energy between E and $E + \mathrm{d}E$, $k_{ij}(E)$ is the unimolecular rate coefficient for isomerization from well j to well i, $k_{\mathrm{d}i}(E)$ and $k_{\mathrm{p}i}(E)$ are the dissociation rate coefficients from well i to $C_3H_3 + C_3H_3$ and to phenyl + H, respectively; n_{R} and n_m are the number densities, respectively, of the deficient and excess reactants (explained below), and $K_{\mathrm{eq}i}$ is the equilibrium constant for the recombination of $C_3H_3 + C_3H_3$ into well i. The function $F_i(E)$ is the equilibrium energy distribution in well i at temperature T,

$$F_i(E) = \rho_i(E)\mathrm{e}^{-\beta E}/Q_i(T) \quad (5)$$

where $Q_i(T)$ is the vibrational−rotational partition function for the ith well. Of course, many of the rate coefficients appearing in eq 4 are taken to be identically zero in our calculations. In fact, the only rate coefficients that are not zero are the ones that have "reactants" and "products" directly connected by one of the transition states shown in Figure 1.

For the present investigation we consider only cases where nitrogen (N_2) is the bath gas. Moreover, to produce a linear master equation, we restrict our attention to a hypothetical, *experimentally unrealizable*, physical situation in which we envision two types of propargyl radicals, one in great excess and the other deficient in concentration. To make the situation concrete, one could think of the "excess" propargyl radicals (i.e., the ones that are present in more than sufficient quantities to convert all the deficient ones to products) as having their central carbon atoms replaced by a ^{13}C atom, although such an artifice is not really necessary. In fact, there does not need to be any real physical basis for distinguishing between the two types of propargyls. When we perform the "experiment", i.e., let the propargyl radicals react, if two "excess" propargyl radicals react with each other, we replace them immediately so that n_m, the number density of the "excess" propargyls, remains constant. Therefore, our experimental situation is such that

$$n_{\mathrm{N2}} \gg n_m \gg n_{\mathrm{R}} \quad (6)$$

and the master eq 4 is linear. Of course, such an experimental situation cannot be attained in the laboratory. But that is not the point. The important point is that, if it could be realized, we could extract kinetics information in the same way one normally does for radical−molecule reactions. Theoretically, we are not encumbered by experimental limitations. We only have to imagine the situation and calculate the outcome. The thermal rate coefficients and product distributions are the same as those for any physically realistic, inherently nonlinear, experiment as long as both sets of results are interpreted correctly.

To complete the problem specification it is necessary to add an equation for n_{R},

$$\frac{\mathrm{d}n_R}{\mathrm{d}t} = \sum_{i=I,II,V}\int_{E_{0i}}^{\infty} k_{\mathrm{d}i}(E)n_i(E)\mathrm{d}E - n_{\mathrm{R}}n_m\sum_{i=I,II,V} K_{\mathrm{eq}i}\int_{E_{0i}}^{\infty} k_{\mathrm{d}i}(E)F_i(E)\,\mathrm{d}E \quad (7)$$

The terms in eq 7 represent the rates of dissociation and recombination between $C_3H_3 + C_3H_3$ and wells I, II, and V, as shown in Figure 1. In deriving eqs 4 and 7, it was assumed that the reactants are maintained in a thermal distribution throughout the course of the reaction even though the complexes are not. Such an assumption is consistent with the inequalities 6.

To solve eqs 4 and 7, it is convenient to cast them in a different form. In so doing we follow closely the development given in our previous work,[41] leaving out the details. First, let $x_{\mathrm{R}}(t) = n_{\mathrm{R}}(t)/n_{\mathrm{R}}(0)$, $x_i(E,\ t) = n_i(E,\ t)/n_{\mathrm{R}}(0)$, and $y_i(E,t) = x_i(E,t)/f_i(E)$, where $f_i^2(E) = F_i(E)Q_i(T)$. Then, after approximating the integrals in eqs 4 and 7 as discrete sums with an energy spacing δE, we can express them in the concise form (using Dirac notation)

$$\frac{\mathrm{d}}{\mathrm{d}t}|w(t)\rangle = G|w(t)\rangle \quad (8)$$

where $|w(t)\rangle$ is the vector of unknowns,

$$|w(t)\rangle \rightarrow \left[y_1(E_{0l}), ... y_1(E_l), ... y_i(E_{0i}), ...y_i(E_l), ..., \left(\frac{n_m}{Q_{\mathrm{R}m}\delta E}\right)^{1/2} x_{\mathrm{R}}\right]^T, \quad (9)$$

G is a real, symmetric matrix, and E_l in ref 9 is the energy of the lth gridpoint. Clearly, $|w(t)\rangle$ has $1 + \sum_{i=I}^{VII} N_i$ components, where N_i is the number of grid points in the energy space of well i.

From the solution vector it is relatively straightforward to extract information about the relative populations $x_R(t)$, $X_i(t)$, and $x_p(t)$, where

$$X_i(t) = \int_{E_{0i}}^{\infty} x_i(E, t)\, dE \qquad i = I, ..., M \tag{10}$$

and

$$x_p(t) = 1 - x_R(t) - \sum_{i=I}^{M} X_i(t) = \frac{n_H(t)}{n_R(0)} = \frac{n_{phenyl}(t)}{n_R(0)} \tag{11}$$

and $x_p(t)$ is the fraction of the initial reactant concentration, $n_R(0)$, that has formed bimolecular products at time t. As in previous work, it is useful in interpreting our results to compute a time-dependent rate coefficient $k(T, p, t)$,

$$k(T, p, t) = -\frac{1}{n_m x_R(t)} \frac{dx_R(t)}{dt} \tag{12}$$

If x_R ultimately goes to zero (it does) and decays exponentially in time, $k(T,p,t) = k(T,p)$ is constant in time, and we have a "good" rate coefficient. In cases where there are multiple-exponential decays, we characterize the rate using eq 12 at the time when $x_R(t)$ has dropped to a value of 1/2. Similarly, to avoid any ambiquity that might occur in the product distribution, the branching fractions are defined as

$$\alpha_i = X_i(\tau) \qquad i = I, ..., M$$
$$\alpha_{bi} = x_p(\tau) \tag{13}$$

where τ is the time when $x_R(\tau)$ has dropped to a value $x_R(\tau) \approx 0.01$, α_i is the branching fraction for stabilization into well i, and α_{bi} is the branching fraction for formation of bimolecular products.

In the present investigation it was necessary to solve eq 8 by two different methods. The first method is our method of choice. It is the one we have used in our previous work[41−43] and the one employed by most other investigators.[46−50,53,54] Equation 8 has the solution

$$|w(t)\rangle = \sum_{j=1}^{N_I+...N_M+1} e^{\lambda_j t} |g_j\rangle \langle g_j|w(0)\rangle \tag{14}$$

where λ_j and $|g_j\rangle$ are the $1 + \sum_{i=I}^{M} N_i$ (negative) eigenvalues and eigenvectors of G, and $|w(0)\rangle$ corresponds to $x_R(0) = 1$. Equation 14 can be thought of as an expansion in the normal modes of relaxation of G.[43,57−60] The slow modes, i.e., the ones corresponding to the algebraically largest eigenvalues (the ones with the smallest absolute values), describe "chemical" processes, whereas the others describe intermolecular energy transfer. Typically there is one chemically significant eigenvalue/eigenvector pair for each transition state in the problem, consistent with the idea that a transition state is a "bottleneck" for reaction in configuration space. In the present case, there are eight chemically significant eigenvalues, with the transition states marked 1a, 1b, and 1c in Figure 1, all correlating with a single eigenvalue. It is instructive and useful to discuss our results in terms of these eigenvalues and eigenvectors. Moreover, eq 12 indicates that a "good" rate coefficient exists only when $x_R(t)$ is governed by a single eigenvalue/eigenvector pair. In such cases, $x_R(t)$ falls and the products rise with the same time constant. To diagonalize G and thus express the solution vector $|w(t)\rangle$ as eq 14, we use the DSYEV routine from LAPACK.[61]

At low temperatures (in the present case for $T < 1000$ K) it frequently occurs that eigenvalues that are very small in magnitude are not computed accurately by the diagonalization routine. In fact, in many instances they turn out positive. Although such results usually do not affect the value of the thermal rate coefficient (for reasons that will become obvious below), they do impact the product distribution, at least for the minor components. Consequently, for $T < 1000$ K, we integrate eq 8 directly using the stiff ODE integrator VODE.[62] This method has been used previously by Miller and Chandler[55,56] in solving the master equation for overtone dissociation and isomerization problems. It is much more robust than the eigenvector expansion method, but it is slightly more time-consuming. However, it may well be possible to reduce the computing time by adjusting the error control, a tactic that we have not yet attempted.

All of the master equation calculations in the present work were done with VARIFLEX,[45] into which both the VODE and eigenvector expansion methods have been incorporated. For simplicity, a single-exponential down model was used for the energy transfer function with $\langle \Delta E_d \rangle = 500$ cm^{-1}.

Results and Discussion

Both the product distribution and the thermal rate coefficient $k(T,p)$ are of considerable practical and theoretical interest. Consequently, we discuss both in some detail below. Let us begin with the rate coefficient.

The Thermal Rate Coefficient. Figure 4 is a plot of the thermal rate coefficient versus temperature for a series of pressures ranging from $p = 1$ Torr to $p = 100$ atm. Also shown on the plot are $k_\infty(T) = k_{1a\infty} + k_{1b\infty} + k_{1c\infty}$, the "high-pressure limit" of the recombination rate coefficient, and $k_0(T)$, the rate coefficient in the zero-pressure (collisionless) limit. There are three important temperature regimes.

(i) $T \leq 500$ K. In this temperature range, $k_0(T) \approx k_\infty(T)$, and the rate coefficient for all intervening pressures is the same. This behavior indicates that any C_6H_6 complex that is formed from $C_3H_3 + C_3H_3$ ultimately ends up as some product, and very few such complexes redissociate back to reactants. This is not surprising in view of the character of the potential energy surface (Figure 1), i.e., the rearrangement barriers all lie well below the entrance-channel energy so that any complex that is not stabilized can go on to phenyl + H with relative ease. However, it is interesting that very little phenyl + H is actually formed under these conditions, even at $p = 1$ Torr.

(ii) 500 K < T < 2000 K. This is the temperature regime of most practical interest, because virtually all combustion takes place at these temperatures. In this range, k is a function of both pressure and temperature. Increased pressure results in higher collision rates, which in turn increase the stabilization rates of the various C_6H_6 isomers. As expected, $k(T,p)$ is a monotonically increasing function of pressure in this regime. In principle, for ordinary reactions $k(T,p)$ could increase with pressure until it approaches $k_\infty(T)$. However, reaching such a limit is problematic at high T, even though, for $p = 100$ atm, $k(T,p) \approx k_\infty(T)$ up to $T \approx 1000$ K.

(iii) $T \geq 2000$ K. This is an extremely intriguing regime, one that we have also identified in our previous investigations of the $C_2H_5 + O_2$ and $C_2H_3 + C_2H_2$ reactions,[41−43] although the temperature at which it begins is highly reaction dependent. In the present case, for $T \geq 2000$ K, $k(T,p) \approx k_0(T)$ *independent of pressure*, even though the intermediate complexes may suffer numerous collisions. This situation occurs when activating collisions, those with $\Delta E \geq 0$, become competitive with

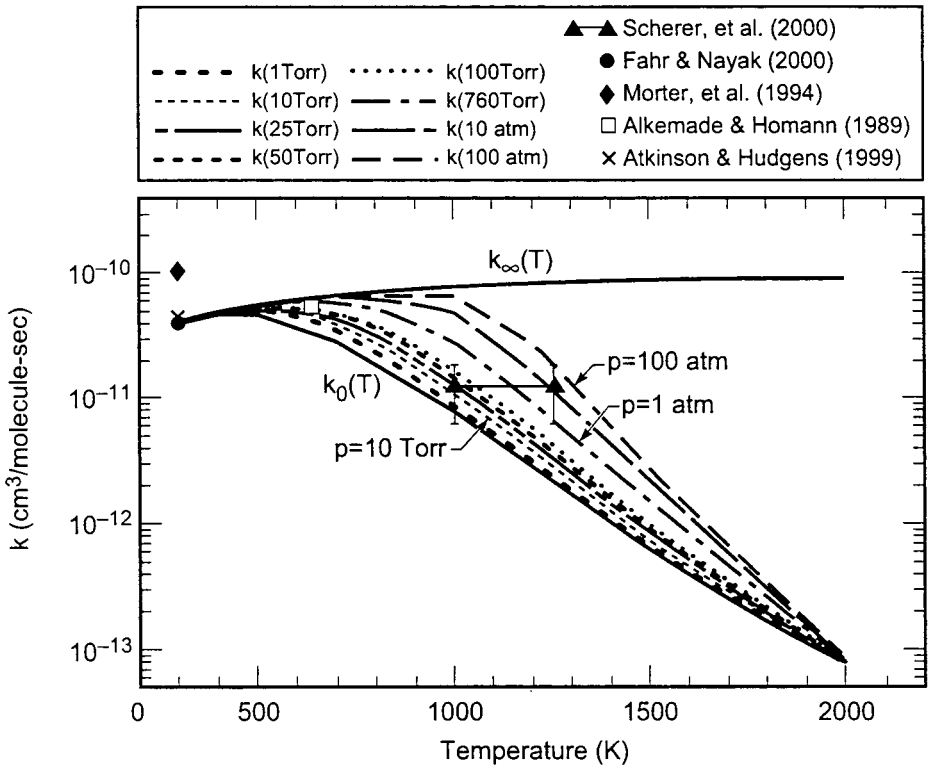

Figure 4. Plot of $k(T)$ for various pressures. The experimental results are due to Fahr and Nayak,[40] Atkinson and Hudgens,[29] Morter et al.,[69] Scherer et al.,[64] and Alkemade and Homann.[63]

deactivating collisions ($\Delta E < 0$) at energies very high in the energy manifolds of the various isomers shown in Figure 1. Then the condition, $\langle \Delta E \rangle = 0$ (where $\langle \Delta E \rangle$ is the average energy transferred in all collisions, both activating and deactivating), can occur at similarly high energies. The energy at which $\langle \Delta E \rangle$ goes to zero can be viewed as a stabilization bottleneck, since a complex with such an energy that suffers a deactivating collision is more likely in the next collision to be reactivated than it is to lose more energy. If a dissociation or isomerization transition state lies at an energy in the vicinity of the $\langle \Delta E \rangle = 0$ energy, such a dissociation or isomerization serves as a "sink" for complexes, and no stabilization occurs. For $T \geq 2000$ K in the $C_3H_3 + C_3H_3$ reaction, because of this phenomenon, stabilization cannot occur in *any* of the wells. Actually, such a condition is reached at different temperatures for each of the wells individually, but this becomes apparent only when one looks at the product distributions. We shall refer to the condition reached here at 2000 K as the "stabilization limit" (i.e., for all the wells) and the temperature at which it occurs as the "coalescence temperature."

A particularly surprising result is the precipitous drop off of $k(T,p)$ with temperature, independent of pressure, between room temperature and 2000 K. This is a consequence of the tight transition states along the reaction path between $C_3H_3 + C_3H_3$ and benzene, particularly TS-4 and TS-7. The theoretical predictions are in good agreement with the room-temperature rate coefficient of Fahr and Nayak (they were constrained to be) and are consistent with the slight increase of k with temperature implied by the result of Alkemade and Homann,[63] whose experiments were performed between 2 and 4 Torr. Of course, the latter agreement can be achieved only with a value of $k_\infty(T)$ that increases with temperature.

High-temperature experimental results for $k(T,p)$ are extremely scarce. In fact, the only one that we could find is the very recent investigation by Scherer et al.[64] in which $k(T,p)$ was obtained by indirect means in a shock tube experiment at pressures of approximately 1−2 atm. These results are also plotted in Figure 4. The agreement between our theoretical predictions and the measurement of Scherer et al. is quite good. Nevertheless, it would be extremely valuable to have more high-temperature measurements of $k(T,p)$ (with which to compare the theory) in order to confirm or deny the large decay of the rate coefficient at these temperatures.

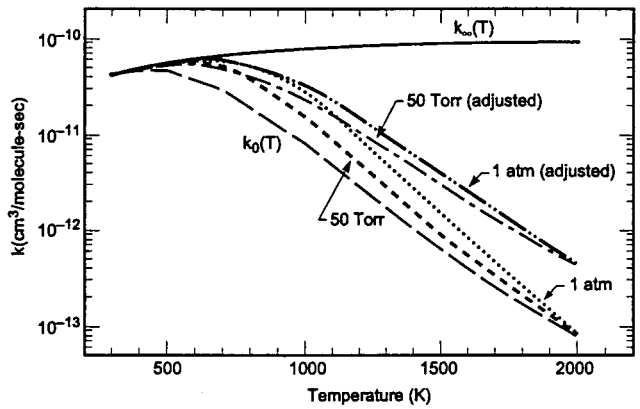

Figure 5. Influence of reducing E_{04a}, E_{04b}, and E_{07} by 10 kcal/mol on $k(T,p)$ at $p = 50$ Torr and $p = 1$ atm.

To illustrate the influence of the rearrangement barriers on $k(T,p)$, we have plotted in Figure 5 the rate coefficients at 50 Torr and 1 atm for two cases: (1) the BAC-MP4 results as shown in Figure 4, and (2) a case where E_{04a}, E_{04b}, and E_{07} (the threshold energies for TS-4a, TS-4b, and TS-7) were reduced by 10 kcal/mol.

The two sets of rate coefficients begin to deviate at roughly 800 K and differ by a factor of 6 at the coalescence temperature ($T = 2000$ K). Even with such a large modification to the barrier

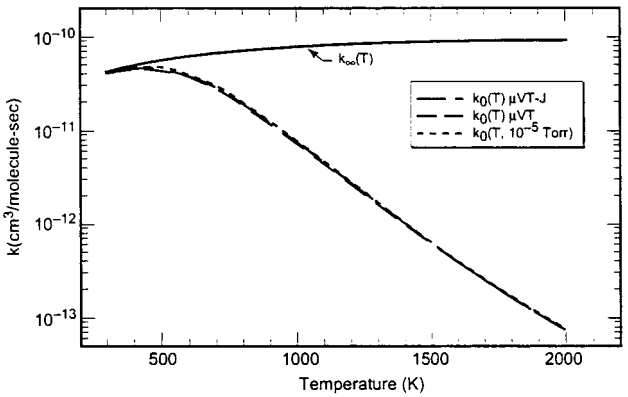

Figure 6. Effect of various ways of handling angular momentum on $k_0(T)$, the zero-pressure rate coefficient.

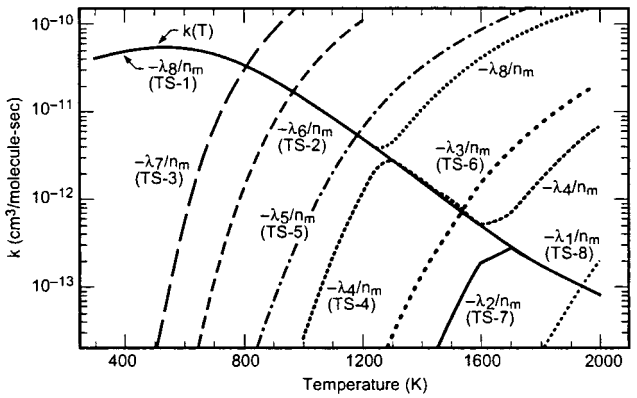

Figure 7. Rate coefficient $k(T,p)$ and eigenvalue curves $-\lambda_i/n_m$ (i = 1, ..., 8) for the chemically significant eigenvalues at $p = 50$ Torr.

heights, probably beyond the error limits of the BAC-MP4 calculations, $k(T,p)$ still drops off quite dramatically at high temperature.

It is possible to check the impact of certain rotational effects in our calculations, namely those associated with rotational channel switching.[1,65,66] Such effects are expected to be most pronounced at the collisionless limit. In Figure 6 we plot $k_0(T)$ from μVT (microcanonical variational transition-state theory) and μVT-J, along with $k(T)$ for $p = 10^{-5}$ Torr. These represent three distinct ways of handling molecular rotation. In μVT there is one dividing surface for each of the loose transition states at every value of E, and E is conserved in going from one transition state to another. In μVT-J there is a different dividing surface for every E, J combination for each loose transition state, and both E and J are conserved between transition states. The rate coefficient at 10^{-5} Torr is effectively at the collisionless limit. In this calculation we treat angular momentum as described in the Theory section, i.e., a μVT-J treatment of the loose transition states, but only E is conserved in going from one transition state to another. These three rate coefficients are indistinguishable on the plot, and thus it is fair to say that angular momentum conservation is not a dominant factor in determining $k(T,p)$.

The failure of J conservation to have an impact on $k_0(T)$ is relatively easy to understand, at least qualitatively. At low temperatures, loose transition states have dividing surfaces located at relatively large fragment separations, and the dividing surface positions indeed are controlled by centrifugal barriers. However, at such low temperatures the rearrangement transition states do not have much of an effect on $k_0(T)$, because they lie so low in energy. Consequently, angular momentum conservation is not important. As temperature is increased and the tight transition states begin to affect $k_0(T)$, the loose dividing surfaces move to smaller fragment separations, where centrifugal barriers are no longer the dominant effect, and again angular momentum conservation is unimportant.

It is particularly interesting and informative to consider our results in terms of the eigenvalues and eigenvectors of G. There are eight chemically significant ones. These in fact correspond to the slow normal modes of relaxation of the entire system. Because our mathematical model does not allow the bimolecular products, phenyl + H, to recombine, all the eigenvalues are negative. Let us define λ_1 to be the algebraically largest eigenvalue (the least negative one), λ_2 to be the next largest one, and so on. The corresponding eigenvectors are $|g_1\rangle$, $|g_2\rangle$, etc. If we had allowed for the reverse process, phenyl + H $\rightarrow$ benzene, there would be another eigenvalue, $\lambda_0 = 0$, corresponding to complete thermal and chemical equilibrium. If one thinks of each of the terms in eq 14 as propagating sequentially in time, it is conceptually easy to envision each chemically significant eigenpair as a mini chemical reaction. Each eigenvector individually has the conservation property[67,68] (taking into account eq 11)

$$(\Delta x_R + \sum_{i=I}^{VII} \Delta X_i + \Delta x_p)_j = 0 \qquad j = 1, ..., 8 \qquad (15)$$

where Δ indicates the change in population that accompanies the propagation of the jth eigenpair from $t = 0$ to $t = \infty$. Note that the magnitudes of the terms in eq 15, i.e., the overall scale, is different for different eigenvectors because the scalar coefficient $\langle g_j|w(0)\rangle$ is different in each case. If only one term in eq 15 is positive (the product) and one is negative (the reactant), that eigenpair indeed represents a simple chemical reaction as we normally think of it, with one reactant (or set of reactants) and one product (or set of products). In such cases

$$-\lambda_i = k_f + k_r \qquad (16)$$

where k_f and k_r are the forward and reverse rate coefficients for the reaction in question; $-\lambda_i$ is called the "fundamental relaxation rate"[57−60] for that reaction. The equilibrium condition, $k_f/k_r = K_{eq}$, allows determination of k_f and k_r individually. (It should be noted that, in case of the pseudo first-oder process involving the reactants, k_f and K_{eq} each should be multiplied by n_m in eq 16 and the equilibrium condition.) However, the situation can become much more complex than that just described, with eq 15 having several negative terms and several positive terms in the most complicated situations.

To help understand how the considerations just described relate to the present analysis, consider Figure 7. If $k(T,p)$ is governed by a single eigenvalue of G, which is the only way that a "good" rate coefficient can exist, one obtains from eq 12

$$k(T,p) = -\lambda_i/n_m \qquad (17)$$

for i corresponding to one of the eight chemically significant eigenvalues. Figure 7 shows values of $-\lambda_i/n_m$ for $i = 1, ..., 8$ and $k(T,p)$ for a pressure of 50 Torr, where the eigenvalue curves are labeled by their size at low temperature. As temperature is increased, $k(T,p)$ first coincides with $-\lambda_8/n_m$, then $-\lambda_4/n_m$, and finally $-\lambda_2/n_m$, with crossings of other eigenvalue curves along the way and "avoided crossings" [41−43] when $k(T,p)$ switches from one eigenvalue curve to another.

At low temperature it is relatively easy to identify one transition state with each chemically significant eigenvalue, consistent with the notion introduced in the Theory section that

the slow modes of relaxation correspond to bottlenecks in the overall relaxation process. There is the exception to this rule that TS-1a, TS-1b, and TS-1c all correlate with one eigenvalue, λ_8. The transition states that correlate with the various eigenvalues are shown on the diagram. As temperature is increased, and various crossings and avoided crossings occur, the eigenvalue curves are distinguished in the plot by their transition states, not by their relative magnitudes at a specific T. To identify a transition state with an eigenvalue, we modified a property (usually its barrier height) for each transition state individually and inquired as to how the eigenvalue spectrum was changed. Normally, one λ_i was changed substantially with the others remaining relatively constant. However, in the vicinity of crossings and avoided crossings, it sometimes happened that 2 or 3 λ_i could change when a barrier height was changed. This normally happened when the eigenvalues were chemically coupled in some way, e.g., representing competing isomerization paths for a single complex. In all cases, when such a situation occurred, one λ_i was changed by a significantly larger fraction than the others, and that eigenvalue was identified with the transition state under investigation. At temperatures above a crossing or avoided crossing, it is again relatively easy to make the identifications, at least until an eigenvalue merges with the "continuum" of energy-transfer eigenvalues above $-\lambda_i/n_m \approx 10^{-9}$ cm^3/molecule-s.

At temperatures below the $k(T,p)$ curve in Figure 7, where the eigenvalues are distinct in magnitude from each other, $-\lambda_i$ can frequently be identified as the fundamental relaxation rate for a simple isomerization or dissociation/recombination reaction. The reactants and products of such reactions are the chemical species directly connected by the transition state corresponding to that eigenvalue, i.e., these are the only terms in eq 15 that are nonzero. For example λ_1 corresponds to the benzene → phenyl + H reaction, λ_2 to fulvene ↔ benzene, λ_3 to fulvene ↔ 2-ethynyl−1,3-butadiene, etc. The situation with some of the other eigenvalues is slightly more complicated in that multiple reactants or products are involved, but the basic idea should be clear.

As the temperature increases the situation becomes more interesting, particularly in the case of avoided crossings, where two eigenvalue curves approach each other, $k(T,p)$ jumps from one curve to the other, and the curves then diverge. In such cases there is a narrow temperature region in which Δx_R in eq 15 is significantly negative for both eigenvectors involved, and $x_R(t)$ exhibits biexponential decays corresponding to the two eigenvalues. For example, near $T = 1200$ K the $k(T,p)$ curve jumps from $-\lambda_8/n_m$, corresponding to TS-1, to $-\lambda_4/n_m$, corresponding to TS-4. Between 1200 and 1600 K $x_R(t)$ is controlled by TS-4, even though this transition state is relatively far removed from the reactants in configuration space. There is a similar jump from $-\lambda_4/n_m$ to $-\lambda_2/n_m$(TS-7) between 1600 and 1700 K. The rate coefficient $k(T,p) = -\lambda_2/n_m$ for $T \geq 1700$ K, at least for $p = 50$ Torr. The situation is similar at other pressures as long as collisions are a major factor in determining the rate coefficient. Changing the pressure does not change the roles of the various transition states and eigenpairs, but it can have an effect on the precise temperatures at which the crossings and avoided crossings occur.

The Product Distributions. It is our hope that the present investigation will spawn a host of new experiments that will seek to confirm or deny our theoretical predictions. There is a dearth of such experiments at the present time, both for the rate coefficient and the product distribution. To this end, we include in the present article a large number of predictions for product distributions at various temperatures and pressures. These are contained in Figures 8 through 16, which are plots of α_{bi} and α_i (i = I, ... VII) defined by eq 13, as a function of pressure, 1 Torr $\leq p \leq$ 10 atm, for a series of temperatures (295, 500, 650, 800, 1000, 1200, 1500, 1700, and 2000 K).

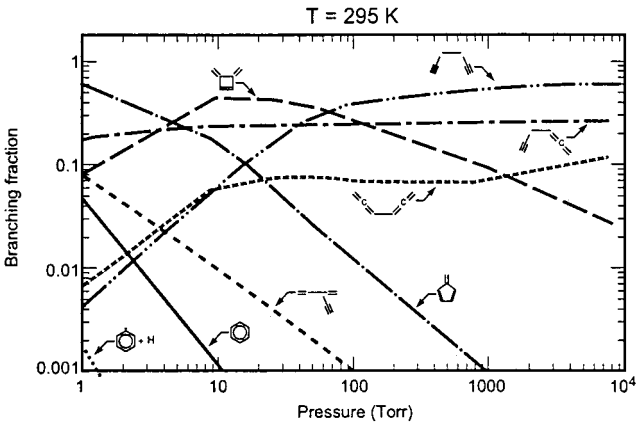

Figure 8. Product distribution as a function of pressure at $T = 295$ K.

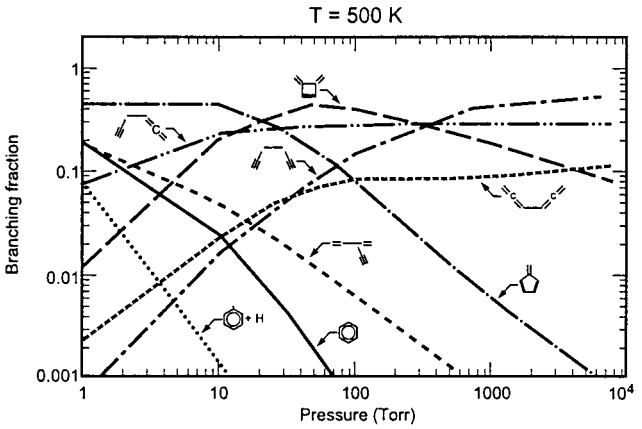

Figure 9. Product distribution as a function of pressure at $T = 500$ K.

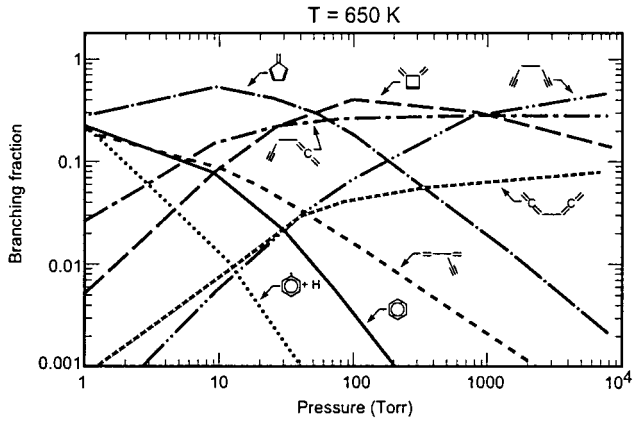

Figure 10. Product distribution as a function of pressure at $T = 650$ K.

First, consider the low-temperature regime, which we shall take to be $T \leq 800$ K, although the precise temperature range is not really well defined. In this regime, the trends in the product distributions as a function of pressure are as one might expect. At very low pressures, no stabilization can occur, and the only product is phenyl + H. As pressure is increased, the first stabilization products one sees are the ones with the deepest wells: benzene, fulvene, and 2-ethynyl−1,3-butadiene. As

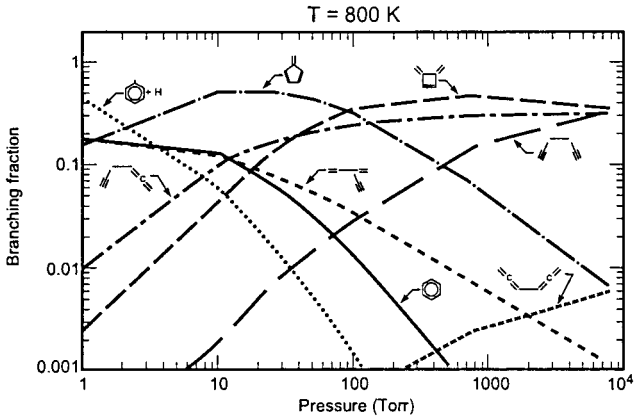

Figure 11. Product distribution as a function of pressure at $T = 800$ K.

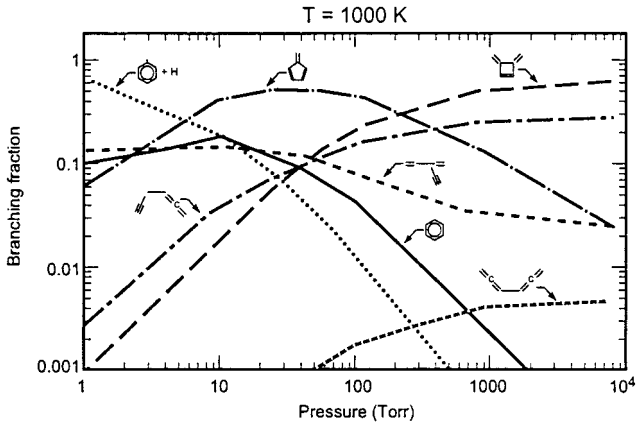

Figure 12. Product distribution as a function of pressure at $T = 1000$ K.

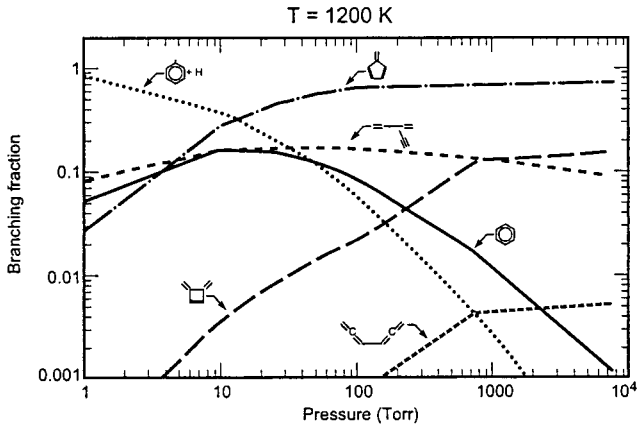

Figure 13. Product distribution as a function of pressure at $T = 1200$ K.

pressure is increased further, these products are supplanted by those that occur earlier along the reaction path shown in Figure 1. By the time we reach $p = 10$ atm at $T = 295$ K, the only significant products are those that are formed directly from $C_3H_3 + C_3H_3$, i.e., well I, well II, and well V. In effect, the high-pressure-limit product distributions for these recombination reactions have been reached at this point. The major change brought about by an increase in temperature in this regime is that the low-pressure products tend to persist to higher pressures.

As discussed in the Theory section, we constrained $k_{1a\infty}$, $k_{1b\infty}$, and $k_{1c\infty}$ to reflect the product distribution determined by Fahr and Nayak at $T = 295$ K and $p = 50$ Torr. However, because the isomerization from well I (1,5-hexadiyne) to well II, and

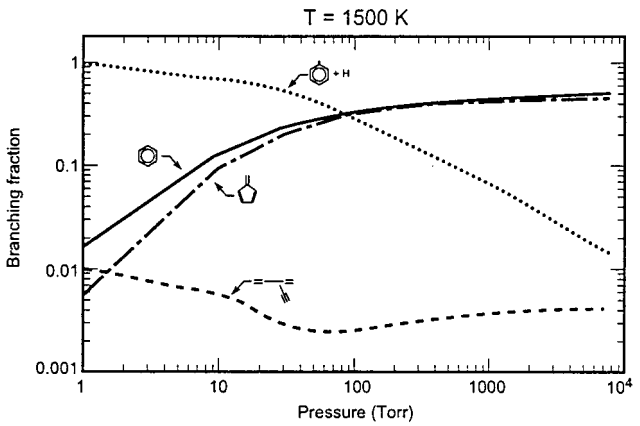

Figure 14. Product distribution as a function of pressure at $T = 1500$ K.

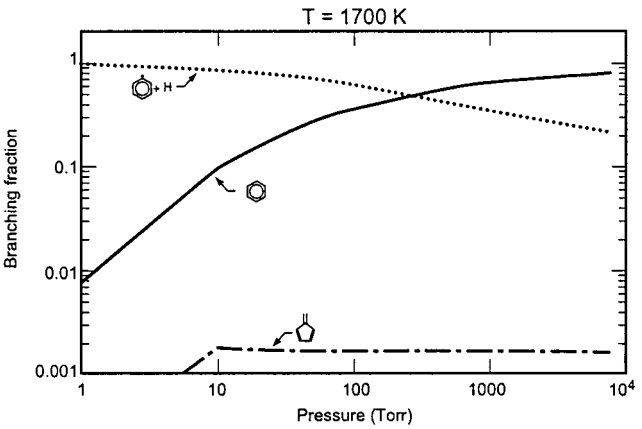

Figure 15. Product distribution as a function of pressure at $T = 1700$ K.

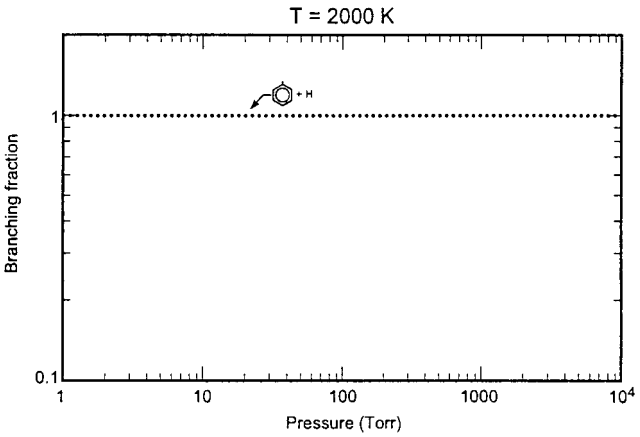

Figure 16. Product distribution as a function of pressure at $T = 2000$ K.

on to well III (dimethylene-cyclobutene) occurs so readily, the master equation results do not produce the intended effect. Such a result could possibly be a consequence of an error in the BAC-MP4 threshold energy E_{02}. One might naturally ask what change in E_{02} would bring the master equation results in line with the Fahr and Nayak measurements. This question is answered in Figure 17. An increase of 4 to 5 kcal/mol would increase α_I to a value above 0.5, which is probably within the error limits of the experimental value of $\alpha_I = 0.60$. Figure 17 also shows that the increase in α_I as E_{02} is raised occurs at the expense of α_{III} and that an increase in E_{02} of 10 kcal/mol causes α_I effectively to reach its high-pressure limit.

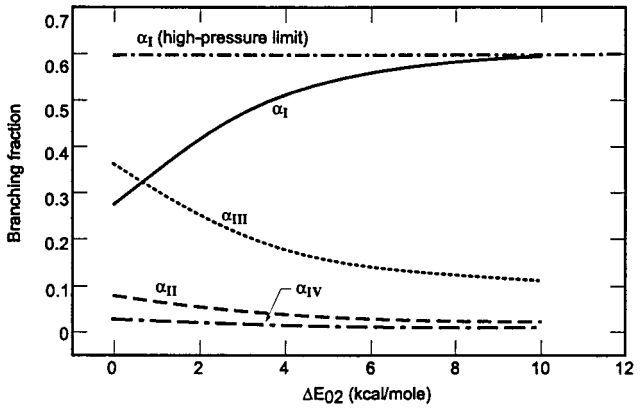

Figure 17. Effect of increasing E_{02} on the product distribution at $T = 295$ K and $p = 50$ Torr.

At $T \approx 650$ K Alkemade and Homann[63] detected the products (roughly in order of importance) 1,2 hexadiene-5-yne (well V), benzene (well VII), 1,3-hexadiene-5-yne (not shown in Figure 1), 1,5-hexadiyne (well I), and 1,2,4,5-hexatetraene (well II) at pressures between 2 and 4 Torr. These results are in conflict with the master equation predictions shown in Figure 10. Most of the discrepancy may be due to the way we constrained our values of $k_{1a\infty}$, $k_{1b\infty}$, and $k_{1c\infty}$ at $T = 295$ K, forcing head-to-head recombination of the propargyl radicals to be the dominant reaction mechanism. Alkemade and Homann's results strongly imply that head-to-tail recombination is dominant at $T \approx 650$ K, at least if the BAC-MP4 PES is correct. For Alkemade and Homann's result to be compatible (on the basis of the BAC-MP4 potential) with that of Fahr and Nayak, on whose experiments our values of $k_{1\infty}$ are based, would require a crossing of $k_{1a\infty}$ and $k_{1c\infty}$ between 295 and 650 K. A particularly interesting result from Alkemade and Homann's experiment is the detection of 1,3-hexadiene-5-yne as a product. The BAC-MP4 potential shows that this C_6H_6 isomer is accessible by isomerization from well V.[22,23] However, the V → VI path is favored over this isomerization by about 25 kcal/mol. As noted by Melius et al.,[23] earlier thermal pyrolysis experiments favor the V → VI path over 1,3-hexadiene-5-yne formation. If the 2 isomerization barriers were not so different, the two results might be compatible, since one experiment is thermally activated and the other is chemically activated. It is also not out of the question that an undiscovered path connecting well I or well II to 1,3-hexadiene-5-yne might exist. Such a path could also help to explain the discrepancy.

For temperatures above $T = 800$ K, another factor begins to affect the product distributions: various isomers begin to reach their "stabilization limits." Although 1,5-hexadiyne is one of the dominant products above 1 atm in Figure 11 ($T = 800$ K), its branching fraction drops below the threshold of the plot at 1000 K, a consequence of passing its stabilization limit. Well II (1,2,4,5-hexatetraene) also reaches its stabilization limit at $T \approx 800$ K, but the consequence in this case is that it equilibrates with dimethylene cyclobutene (well III). For $T > 800$ K, well II and well III respond in concert to changes in temperature and pressure.

As temperature increases from 800 to 2000 K, each C_6H_6 isomer in turn reaches its stabilization limit and drops off the subsequent branching fraction plots. Well I reaches its limit between 800 and 1000 K, well V between 1000 and 1200 K, wells II and III between 1200 and 1500 K, and well VI between 1500 and 1700 K. Fulvene reaches its stabilization limit between 1700 and 1800 K, although the 1800 K result is not shown, and benzene drops off the plots between 1800 and 2000 K. For $T \geq 2000$ K, the only significant product is phenyl + H.

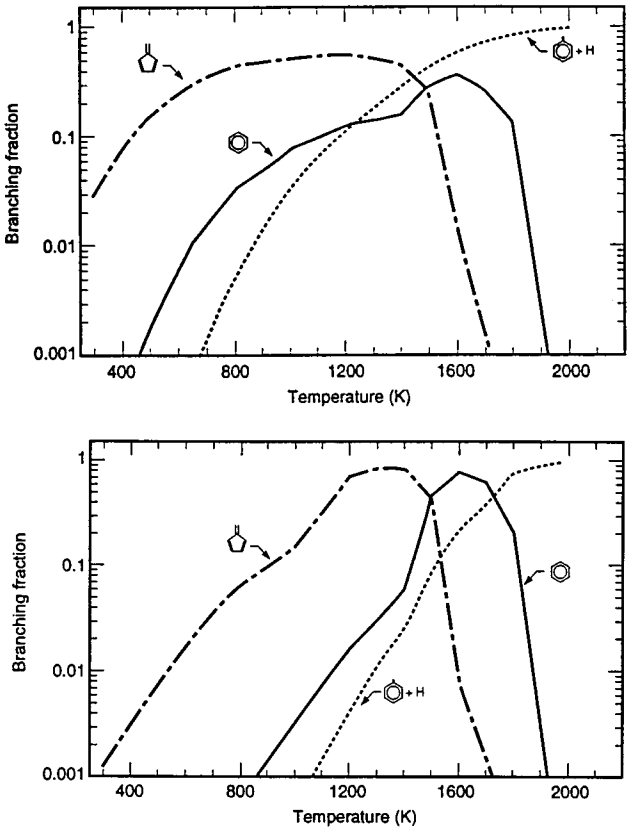

Figure 18. Fulvene, benzene, and phenyl + H branching fractions as a function of temperature for $p = 50$ Torr (a) and $p = 1$ atm (b).

For combustion purposes the important products are fulvene, benzene, and phenyl + H. Their branching fractions are plotted in Figure 18 as a function of temperature for two different pressures. The 50 Torr case is typical of low-pressure flame experiments, and the 1 atm case is intended to represent normal combustion at atmospheric pressure. Decreasing the pressure below 50 Torr increasingly favors phenyl + H; increasing the pressure above 1 atm does not change the results very much. Both α_{IV} and α_{VII} drop off dramatically as the fulvene and benzene stabilization limits are reached; each has also risen rapidly as the isomers preceding it along the reaction path reach their stabilization limits. Note particularly the connection between Figure 7 and Figure 18. At 1200 K the $k(T,p)$ curve in Figure 7 shifts from $-\lambda_8/n_m$ (governed by TS-1) to $-\lambda_4/n_m$ (governed by TS-4). This shift corresponds to the stabilization limits having been reached for all the isomers to the left of TS-4 in Figure 1a. The branching fractions for these species is negligible beyond this temperature, as is clear from Figure 18. A similar shift occurs between 1600 and 1700 K from $k(T,p)$ being governed by $-\lambda_4/n_m$ (TS-4) to $-\lambda_2/n_m$ (TS-7) as fulvene's stabilization limit is reached. The occurrence of stabilization limits triggers the appearance of avoided crossings in Figure 7. Actually, an avoided crossing also indicates a shift in equilibrium in favor of the reactants.[43] For $T \geq 2000$ K, benzene's stabilization limit has also been reached, and the only product is phenyl + H, but its rate of formation is still controlled by the fulvene ↔ benzene isomerization transition state.

It is of interest to examine what happens in the vicinity of a stabilization limit. We shall do this for fulvene. Consider Figure 19, which shows thermal equilibrium energy distributions and $\langle \Delta E \rangle(E)$ at a series of temperatures for well IV. Note that the

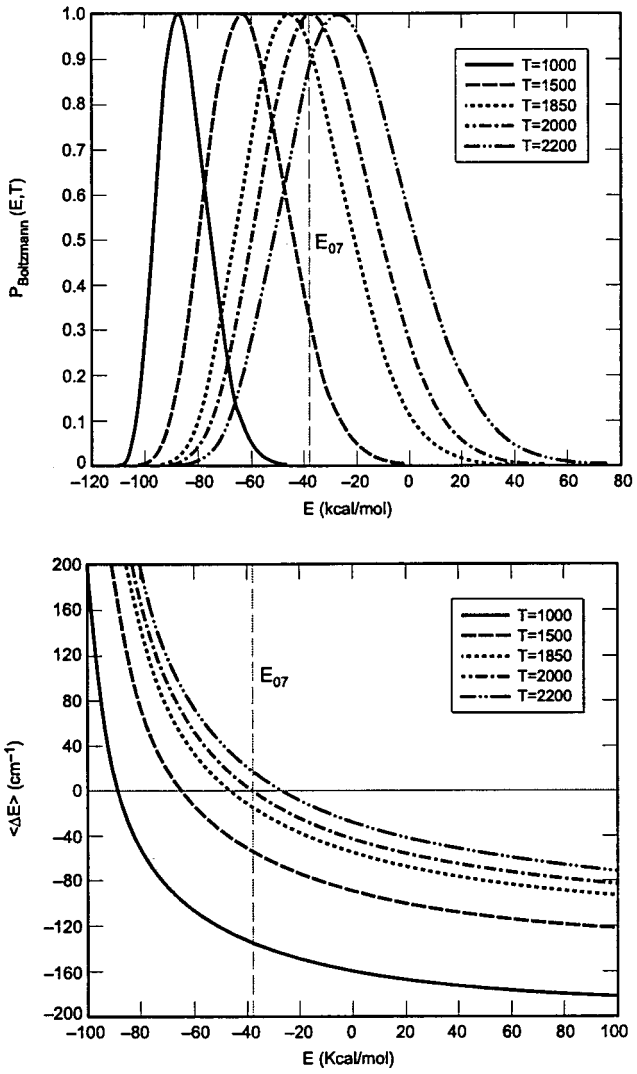

Figure 19. Equilibrium thermal population distributions (a) and $\langle\Delta E\rangle(E)$ (b) for fulvene at selected temperatures, illustrating the "stabilization limit" concept.

$\langle\Delta E\rangle = 0$ point tracks the peak in the thermal energy distribution very closely. At $T = 1000$ K, the peak of the thermal distribution and the $\langle\Delta E\rangle = 0$ point are well below E_{07}, the isomerization limit. Correspondingly, $\langle\Delta E\rangle(E_{07}) \approx -140$ cm^{-1}, i.e., it is significantly negative. As the temperature increases, the thermal distribution shifts to higher energies, and $\langle\Delta E\rangle(E_{07})$ gets increasingly smaller in magnitude until it becomes zero at approximately 2000 K. However, let us focus attention on the curves for $T = 1850$ K, which is just 150 K past the stabilization limit for fulvene described above. At this temperature, the peak in the thermal distribution is at $E \approx -45$ kcal/mol, which is only 7 kcal/mol below the isomerization barrier, and the equilibrium population at $E = E_{07}$ is greater than 90% of the peak. The ultimate function of collisions is to try to establish (or maintain) the equilibrium distribution, but under such conditions, rapid isomerization from a large fraction of the high energy wing causes complexes with those energies to react on a time scale that is much smaller than that for reactant decay. In such cases, where the "stabilization bottleneck" (the $\langle\Delta E\rangle = 0$ point) approaches the isomerization limit, isomerization becomes a nearly infinite sink for complexes, at least as long as chemical equilibrium favors the products. This situation has been described in slightly different terms previously by Miller.[1]

One should not get the idea that every stabilization limit is like the one just described for fulvene. The fulvene ↔ benzene transition state (TS-7) is extremely tight, resulting in relatively slow isomerization rates. As a consequence, a relatively large fraction of the thermal distribution is pushed above the isomerization threshold before the stabilization limit is triggered. In cases where the transition state is much looser (and the isomerization or dissociation rates much faster) than that for fulvene, the stabilization limit occurs much sooner, i.e., when a smaller fraction of the thermal distribution lies above the reaction threshold. The dissociation of benzene to phenyl + H is a good example of the latter case.

An important issue that we have not addressed in the present work is how best to represent the master equation results in terms of phenomenological rate coefficients. For example, consider the temperature range, $1200 < T < 1600$ K. It is clear that one could describe our results in this temperature range as the direct reactions

$$\begin{aligned} C_3H_3 + C_3H_3 &\rightarrow \text{benzene} \\ &\rightarrow \text{fulvene} \\ &\rightarrow \text{phenyl} + H \end{aligned}$$

The master equation results satisfy all the criteria that we can think of to be consistent with a description in terms of these three elementary steps, namely that there is a single time constant for decay of $x_R(t)$ and rise of the products and that the results are independent of the value of n_m (a point that we have not mentioned previously). However, it may be more accurate and more prudent to describe the processes in question as

$$\begin{aligned} C_3H_3 + C_3H_3 &\rightarrow \text{intermediate wells} \\ \text{intermediate wells} &\rightarrow \text{benzene} \\ &\rightarrow \text{fulvene} \\ &\rightarrow \text{phenyl} + H \end{aligned}$$

Here the "intermediate wells" step is intended to be a shorthand representation of a number of intermediate isomerizations (and dissociations) connecting one intermediate well to another and to the indicated products. If such reactions were fast, this latter description of the chemistry would yield results identical to the former. Other scenarios may also lead to ambiguity in the phenomenological description. Ultimately, it may be instructive and practically useful to try to determine how much of each product is formed "directly" and how much is formed "indirectly" in cases such as this one.[43]

Concluding Remarks

In the present article we have discussed at some length the recombination reaction between two propargyl radicals. The principal basis of our discussion is the solution of the time-dependent, multiple-well master equation using the BAC-MP4 potential energy surface and microcanonical (RRKM) rate coefficients calculated from it. Several interesting and important results emerge from the analysis.

1. The thermal rate coefficient $k(T,p)$ drops off precipitously at high temperature, independent of the pressure. One can identify three different temperature regimes for the rate coefficient. (i) $T < 500$ K. In this range $k(T,p) \approx k_\infty(T)$ for all pressures. (ii) 500 K $\leq T < 2000$ K. The thermal rate coefficient here is a function of pressure, as one might normally expect. (iii) $T \geq 2000$ K. At $T = 2000$ K, all the $k(T,p)$ curves coalesce into $k_0(T)$, the rate coefficient at the collisionless limit. This is

the same effect we observed previously in our investigations of the $C_2H_5 + O_2$ and $C_2H_3 + C_2H_2$ reactions. We call this temperature the "coalescence temperature." The situation occurs when all the recombination products reach their "stabilization limits," a condition discussed at length in the paper. Our predictions of $k(T,p)$ are in good agreement with experiment, even though there are not very many experiments with which to compare.

2. The product distributions for $T < 800$ K are relatively easy to understand from conventional reasoning. The importance of a particular product at any pressure is determined by its position along the reaction path and its RRKM lifetime. For $T \geq 800$ K, the various branching fractions $\alpha_i (i = \text{I}, ..., \text{VII})$ begin to drop to zero with relatively small increases in temperature, a consequence of each isomer individually reaching its stabilization limit. For $T > 1200$ K, only fulvene, benzene, and phenyl + H are significant products; above 1700 K only benzene and phenyl + H are important, and above 2000 K the only product is phenyl + H.

3. Interpreting the master equation results in terms of G, the "transition matrix," is very interesting and instructive. Consistent with the idea that the slow normal modes of relaxation correspond to chemical reaction, it is possible to identify each transition state with an eigenvalue/eigenvector pair, usually on a one-to-one basis. However, in the present case the three transition states corresponding to the three ways two propargyl radicals can come together all correlate with one eigenvalue, λ_8. The chemically significant eigenvalues, eight in the present case, are the algebraically largest ones (i.e., the least negative). At sufficiently low temperatures, these eigenvalues are the "fundamental relaxation rates" for particular isomerization or dissociation/recombination reactions, e.g., benzene ↔ fulvene and benzene → phenyl + H. As the temperature increases, crossings and "avoided crossings" of the eigenvalue curves appear, and the simple low-temperature interpretation may no longer apply. In the case of avoided crossings, the $k(T,p)$ curve jumps from one eigenvalue to the other, indicating that control of the overall rate has shifted from one transition state to another. Such shifts are triggered by reaching the stabilization limits (and equilibration) of all the isomers along the reaction path that lie ahead of the transition state to which control is being transferred.

Acknowledgment. This work was supported by the United States Department of Energy, Office of Basic Energy Sciences, Division of Chemical Sciences, Geosciences, and Biosciences.

References and Notes

(1) Miller, J. A. *Proc. Combust. Inst.* **1996**, *20*, 461−480.
(2) Richter, H.; Howard, J. B. *Prog. Energy Combust. Sci.* **2000**, *26*, 565−608.
(3) D'Anna, A.; Violi, A.; D'Allessio, A. *Combust. Flame* **2000**, *121*, 418−429.
(4) D'Anna, A.; Violi, A. *Proc. Combust. Inst.* **1998**, *27*, 425−433.
(5) Faravelli, T.; Goldaniga, A.; Ranzi, E. *Proc. Combust. Inst.* **1998**, *27*, 1489−1495.
(6) Appel, J.; Bockhorn, H.; Frenklach, M. *Combust. Flame* **2000**, *121*, 122−136.
(7) Wang, H.; Frenklach, M. *Combust. Flame* **1997**, *110*, 173−221.
(8) Lindstedt, R. P.; Skevis, G. *Proc. Combust. Inst.* **1996**, 26, 703−709.
(9) Lindstedt, P. *Proc. Combust. Inst.* **1998**, *27*, 269−285.
(10) Dagaut, P.; Cathonnet, M. *Combust. Flame* **1998**, *113*, 620−623.
(11) Westmoreland, P. R.; Dean, A. M.; Howard, J. B.; Longwell, J. P. *J. Phys. Chem.* **1989**, *93*, 8171−8180.
(12) Lamprecht, A.; Atakan, B.; Kohse-Höinghaus, K. *Combust. Flame* **2000**, *122*, 483−491.
(13) Hartlieb, F.; Atakan, B.; Kohse-Höinghaus, K. *Combust. Flame* **2000**, *121*, 610.
(14) Atakan, B.; Hartlieb, A. T.; Brand, J.; Kohse-Höinghaus, K. *Proc. Combust. Inst.* **1998**, *27*, 435.
(15) Douté C.; Delfau, J.-L.; Vovelle, C. *Comb. Sci. Technol.* **1994**, *103*, 153−173.
(16) Pope, C. J.; Miller, J. A., "Exploring Old and New Benzene Formation Pathways in Low-Pressure Premixed Flames of Aliphatic Fuels," *Proc. Combust. Inst.* **2000**, *28*, 1579−1528.
(17) Castaldi, M. J.; Marinov, N. M.; Melius, C. F.; Hwang, J.; Senkan, S. M.; Pitz, W. J.; Westbrook, C. K. *Proc. Combust. Inst.* **1996**, *26*, 693−702.
(18) Marinov, N. M.; Pitz, W. J.; Westbrook, C. K.; Castaldi, M. J.; Senkan, S. M. *Combust. Sci. Technol.* **1996**, *116/117*, 211.
(19) Melius, C. F.; Colvin, M. E.; Marinov, N. M.; Pitz, W. J.; Senkan, S. M. *Proc. Combust. Inst.* **1996**, *26*, 685−692.
(20) Miller, J. A.; Volponi, J. V.; Pauwels, J.-F. *Combust. Flame* **1996**, *105*, 451−461.
(21) Pauwels, J.-F.; Volponi, J. V.; Miller, J. A. *Combust. Sci. Technol.* **1995**, *110−111*, 249−276.
(22) Miller, J. A.; Melius, C. F. *Combust. Flame* **1992**, *91*, 21−39.
(23) Melius, C. F.; Miller, J. A.; Evleth, E. M. *Proc. Combust. Inst.* **1992**, *24*, 621−628.
(24) Davis, S. G.; Law, C. K.; Wang, H. *Proc. Combust. Inst.* **1998**, *27*, 305−312.
(25) Stein, S. E.; Walker, J. A.; Suryan, M.; Fahr, A. *Proc. Combust. Inst.* **1990**, *23*, 85−90.
(26) Slagle, I. R.; Gutman, D. *Proc. Combust. Inst.* **1986**, *21*, 875−883.
(27) Atkinson, D. B.; Hudgens, J. W. *J. Phys. Chem. A* **1999**, *103*, 4242−4252.
(28) Wu, C. J.; Kern, R. D. *J. Phys. Chem.* **1987**, *91*, 6291−6296.
(29) Kern, R. D.; Singh, H. J.; Wu, C. H. *Int. J. Chem. Kinet.* **1988**, *20*, 731−747.
(30) Harkless, J. A. W.; Lester, W. A. *J. Chem. Phys.* **2000**, *113*, 2680−2683.
(31) Bauschlicher, C. W., Jr.; Langhoff, S. R. *Chem. Phys. Lett.* **1992**, *193*, 380−385.
(32) Mebel, A. M.; Lin, S. H.; Yang, X. M.; Lee, Y. T. *J. Phys. Chem. A* **1997**, *101*, 6781−6789.
(33) Madden, L. K.; Mebel, A. M.; Lin, M. C.; Melius, C. F. *J. Phys. Org. Chem.* **1996**, *9*, 801−810.
(34) Bettinger, H. F.; Schreiner, P. R.; Schaeffer, H. F., III; Schleyer, P. V. R. *J. Am. Chem. Soc.* **1998**, *120*, 5741−5750.
(35) Miller, J. A.; Klippenstein, S. J. *J. Phys. Chem. A* **2000**, *104*, 2061−2069.
(36) Varshni, V. P. *Rev. Mod. Phys.* **1957**, *29*, 640−683.
(37) Klippenstein, S. J. *J. Phys. Chem.* **1994**, *98*, 11459−11464 and references therein.
(38) Wardlaw, D. M.; Marcus, R. A. *Chem. Phys. Lett.* **1984**, 110−230.
(39) Wardlaw, D. M.; Marcus, R. A. *J. Chem. Phys.* **1985**, *83*, 3462.
(40) Fahr, A.; Nayak, A. *Int. J. Chem. Kinet.* **2000**, *32*, 118−124.
(41) Miller, J. A.; Klippenstein, S. J.; Robertson, S. H. *J. Phys. Chem. A* **2000**, *104*, 7525−7536 also *J. Phys. Chem. A* **2000**, *104*, 9806 (correction).
(42) Miller, J. A.; Klippenstein, S. J.; Robertson, S. H., "A Theoretical Analysis of the Reaction Between Ethyl and Molecular Oxygen" *Proc. Combust. Inst.* **2000**, *28*, 1479−1486.
(43) Miller, J. A.; Klippenstein, S. J., "The Reaction Between Ethyl and Molecular Oxygen: Further Analysis," *Int. J. Chem. Kinet.* **2001**, in press.
(44) Miller, J. A.; Parrish, C.; Brown, N. J. *J. Phys. Chem.* **1986**, *90*, 3339.
(45) Klippenstein, S. J.; Wagner, A. F.; Dunbar, R. C.; Wardlaw, D. M.; Robertson, S. H.; Miller, J. A., Variflex Version 1.07 mt, December 24, 1999.
(46) Frankcombe, T. J.; Smith, S. C.; Gates, K. E.; Robertson, S. H. *Phys. Chem. Chem. Phys.* **2000**, *2*, 793−803.
(47) Bedanov, V. M.; Tsang, W.; Zachariah, M. R. *J. Phys. Chem.* **1995**, *99*, 11452−11457.
(48) Tsang, W.; Bedanov, V.; Zachariah, M. R. *Ber. Bunsenges. Phys. Chem.* **1997**, 491−499.
(49) Venkatesh, P. K.; Dean, A. M.; Cohen, M. H., Carr, R. W. *J. Chem. Phys.* **1999**, *111*, 8313−8329.
(50) Gates, K. E.; Robertson, S. H.; Smith, S. C.; Pilling, M. J.; Beasley, M. S.; Maschhoff, K. J. *J. Phys. Chem. A* **1997**, *101*, 5765−5769.
(51) Barker, J. R. *Chem. Phys.* **1983**, *77*, 301.
(52) Shi, J.; Barker J. R. *Int. J. Chem. Kinet.* **1990**, *22*, 187.
(53) Blitz, M. A.; Beasley, M. S.; Pilling, M. J.; Robertson, S. A. *Phys. Chem. Chem. Phys.* **2000**, *2*, 805−812.
(54) Tsang, W.; Mokrushin, V., "Mechanism and Rate Constants for 1, 3 Butadiene Decomposition," *Proc. Combust. Inst.* **2000**, *28*, 1717−1723.
(55) Miller, J. A.; Chandler, D. W. *J. Chem. Phys.* **1986**, *85*, 4502.
(56) Chandler, D. W.; Miller, J. A. *J. Chem. Phys.* **1984**, *81*, 445.

(57) Widom, B. *Science* **1965**, *148*, 1555−1560.
(58) Widom, B. *J. Chem. Phys.* **1971**, *55*, 44−52.
(59) Widom, B. *J. Chem. Phys.* **1974**, *61*, 672−680.
(60) Bartis, J. T.; Widom, B. *J. Chem. Phys.* **1974**, *60*, 3474−3482.
(61) Anderson, E.; Bai, Z.; Bishof, C.; Demmel, J.; Dongarra, J.; DuCroz, J.; Greenbaum, A.; Hammerling, S.; McKenney, A.; Ostronchov, S.; Sorensen, *D. LAPACK Users' Guide;* SIAM: Philadelphia, PA, 1992.
(62) Brown, P. N.; Byrne, G. D.; Hindmarsh, A. C. *SIAM J. Sci. Stat. Comput.* **1989**, *10*, 1038−1051.
(63) Alkemade, U.; Homann, K. H. *J. Phys. Chem. (Neue Folge)* **1989**, *161*, 19−34.
(64) Scherer, S.; Just, Th.; Frank, P., "High-Temperature Investigations on Pyrolytic Reactions of Propargyl Radicals," *Proc. Combust. Inst.* **2000**, *28*, 1511−1518.
(65) Troe, J. *J. Chem. Soc., Faraday Trans.* **1994**, *90*, 2303−2317.
(66) Just, Th. *Proc. Combust. Inst.* **1994**, *25*, 687−704,
(67) Montroll, E. W.; Shuler, K. E. *Adv. Chem. Phys.* **1958**, *1*, 361.
(68) Boyd, R. K. *J. Chem. Phys.* **1974**, *60*, 1214−1222.
(69) Morter, C. L.; Farhat, S. K.; Adamson, J. D.; Glass, G. P.; Curl, R. F. *J. Phys. Chem.* **1994**, *98*, 7029−7035.
(70) Ackermann, L.; Hippler, H.; Pagsberg, P.; Reihs, C.; Troe, J. *J. Phys. Chem.* **1990**, *94*, 5247−5251.